NASA Technical Memorandum 102225

A Streamwise Upwind Algorithm Applied to Vortical Flow Over a Delta Wing

Peter M. Goorjian and Shigeru Obayashi, Ames Research Center, Moffett Field, California

October 1989

NASA

National Aeronautics and
Space Administration

Ames Research Center
Moffett Field, California 94035

A STREAMWISE UPWIND ALGORITHM APPLIED TO VORTICAL FLOW OVER A DELTA WING

Peter M. Goorjian and Shigeru Obayashi
NASA Ames Research Center
Moffett Field, California 94035 USA

Summary

Improvements have been made to a streamwise upwind algorithm so that it can be used for calculating flows with vortices. A calculation is shown of flow over a delta wing at an angle of attack. The laminar, thin-layer, Navier-Stokes equations are used for the calculation. The results are compared with another upwind method, a central-differencing method, and experimental data. The present method shows improvements in accuracy and convergence properties.

Introduction

Upwind algorithms are important in computational fluid dynamics for calculations of flows containing shock waves [1]. Some of them are also able to accurately resolve shear layers [2,3]. However, most multidimensional upwind algorithms are first constructed in one dimension and then extended to multidimensions by applying the one-dimensional procedure to each coordinate direction. In comparison, the present method uses the local stream direction and flow velocity to construct the upwinding. Hence the switching of flux evaluations always takes place at sonic values, where the shock waves are located. Therefore this method follows the flow physics more closely and in that respect is analogous to the rotated differencing [4] algorithm developed for the full potential equation.

The present algorithm is an improvement to a streamwise upwind algorithm, which has been applied to steady and unsteady transonic flows over airfoils and wings [5,6,7]. In addition to using rotated differencing to implement upwinding in the streamwise direction, the switching of fluxes across sonic values is smooth and the entropy condition is automatically imposed in a manner similar to Godunov's method. Contact discontinuities are sharply captured [5] and boundary layer profiles are fuller [7] (more accurate) in comparison to a central differencing method for a case of separated flow over a wing.

In the results presented, comparisons are made with the upwind method of Roe [1]. In that method, an entropy correction is needed, which results in a convergence difficulty. The present method does not exhibit that problem. Other features [7] of the present algorithm are that pressure and velocity continuity are enforced in the crossflow direction, and also in the streamwise direction as the velocity approaches zero. These features are adequate for transonic flows without the presence of vortices. However for supersonic flows with vortices, two additional developments were found to be necessary [8]. First, the manner of using the stream direction had to be modified to capture oblique shocks sharply. Second, additional terms were needed to stabilize the calculations. The present algorithm is described in detail.

To demonstrate various capabilities of the present algorithm, the flow was calculated over a delta wing with a leading-edge sweep of 75° at a Mach number of 2.8 and at an angle of attack of 16°. First, a conical flow approximation was used to limit the calculations to two dimensions, so that the influence of grid refinement could be determined. Then full three-dimensional (3D) calculations were performed on a medium-density grid. These computed results were compared with those of other methods and with experimental data.

Governing Equations

The thin-layer Navier-Stokes equations can be written in conservation-law form in a body-conforming, curvilinear, coordinate system (ξ, η, ζ) as follows:

$$\partial_\tau \hat{Q} + \partial_\xi \hat{E} + \partial_\eta \hat{F} + \partial_\zeta \hat{G} = \frac{1}{Re} \partial_\zeta \hat{G}^v \ , \tag{1}$$

where Re is the Reynolds number. The vector of conserved quantities $\hat{Q}$ and the inviscid flux vector $\hat{F}$ are

$$\hat{Q} = \frac{1}{J} \begin{bmatrix} \rho \\ \rho u \\ \rho v \\ \rho w \\ e \end{bmatrix} , \qquad \hat{F} = \frac{1}{J} \begin{bmatrix} \rho \hat{U} \\ \rho u \hat{U} + \eta_x p \\ \rho v \hat{U} + \eta_y p \\ \rho w \hat{U} + \eta_z p \\ \rho H \hat{U} \end{bmatrix} ,$$

where J is the transformation Jacobian, ρ is the fluid density, e is total energy per unit volume, and H is the total enthalpy. The contravariant velocity component $\hat{U}$ is defined as $\hat{U} = \eta_x u + \eta_y v + \eta_z w$. For the ξ and ζ directions, $\hat{E}$ and $\hat{G}$ can be defined similarly. The viscous flux vector $\hat{G}^v$ is given in reference [8]. The pressure p is related to the conservative flow variables $\hat{Q}$ through the equation of state for a perfect gas:

$$p = (\gamma - 1)[e - \frac{\rho}{2}(u^2 + v^2 + w^2)] \ . \tag{2}$$

Also, c is the speed of sound, where $c^2 = \gamma p / \rho$. See reference [8] for the form of equation (1) when the conical-flow approximation is imposed.

Numerical Algorithm

The upwind algorithm is applied to the inviscid fluxes $\hat{E}$, $\hat{F}$, and $\hat{G}$ in equation (1). (The viscous term in equation (1) is discretized by a standard procedure [8], which uses second-order, central-differencing.) The upwind algorithm is described by the following formula for the cell interface flux $\hat{F}$ with a surface vector, $\mathbf{S} = (\eta_x, \eta_y, \eta_z)$,

$$\begin{aligned} \hat{F}(Q_l, Q_r, \mathbf{S}_{j+\frac{1}{2}}) = \frac{1}{2} \frac{|\nabla \eta|}{J} \times \Big\{ & [\, F_l + F_r] + [\, F_l \text{sign}\,(U_l) + s_l \, \Delta^* F_l] \cos^2 \theta_l \\ & - [\, F_r \text{sign}\,(U_r) + s_r \, \Delta^* F_r] \cos^2 \theta_r - |A| \, \Delta Q \, \sin^2 \theta \Big\} \ , \end{aligned} \tag{3}$$

where Q_l and Q_r are left and right states, respectively, and the metric terms η_x, η_y, and η_z are normalized by $|\nabla \eta|$ as $k_x = \eta_x / |\nabla \eta|$, $k_y = \eta_y / |\nabla \eta|$, and $k_z = \eta_z / |\nabla \eta|$. The contravariant velocity $\hat{U}$ is also normalized by $|\nabla \eta|$ and used as $U = k_x u + k_y v + k_z w$. For the first-order-accurate computations, $l = j$ and $r = j + 1$. For higher-order extensions, the MUSCL approach [3,9] is used. Sign(U) equals the sign of U and θ is the rotation angle which will be determined later. The symbol * indicates local sonic values [5].

$$\Delta^* F = \Delta^*(\rho q)\mathbf{e}_s = (\rho^* q^* - \rho q)\mathbf{e}_s \ , \tag{4}$$

$$(q^*)^2 = \left(\frac{2}{\gamma+1}\right)\left(c^2 + \frac{\gamma-1}{2}q^2\right) \ , \qquad \rho^* = \rho\left(\frac{(q^*)^2}{c^2}\right)^{\frac{1}{\gamma-1}} \ , \tag{5}$$

where q is the velocity magnitude and $\mathbf{e}_s = (1, u, v, w, H)^T$ is the sum of the two acoustic wave eigenvectors. Note that equation (4) is based on the rotated difference formula [4,5] for the full potential equation. Equation (4) and the switches s_l and s_r, which will be specified, use the speed q and the Mach number q/c rather than the velocity component U and the Mach number component U/c that many other upwind methods use. With the use of this rotated differencing, the switching of terms at transonic shock waves occurs independently of their alignment to grid lines.

The last term in equation (3) is defined as follows:

$$\begin{aligned} |A|\Delta Q &= |U|\Delta Q + (c - |U|)\left[\frac{\Delta p}{c^2}\mathbf{e}_s + \rho \Delta U \, \mathbf{e}_d\right] \\ &= \frac{\Delta p}{c}\mathbf{e}_s + \rho c \Delta U \, \mathbf{e}_d + \left(\Delta\rho - \frac{\Delta p}{c^2}\right)|U|\,\mathbf{e}_e + \rho\,|U|\,\mathbf{e}_v \ . \end{aligned} \tag{6}$$

The variables in equation (6) are averaged between the left and right states, except when they follow Δ. Then, for example, $\Delta Q = Q_r - Q_l$. Also, $\mathbf{e}_d = (0, k_x, k_y, k_z, U)^T$, which is the difference of the two acoustic wave eigenvectors, $\mathbf{e}_e = (1, u, v, w, q^2/2)^T$ and $\mathbf{e}_v = (0, e_{v2}, e_{v3}, e_{v4}, e_{v5})^T$. Here, $e_{v2} = \Delta u - k_x \Delta U$, $e_{v3} = \Delta v - k_y \Delta U$, $e_{v4} = \Delta w - k_z \Delta U$, and $e_{v5} = u e_{v2} + v e_{v3} + w e_{v4}$. In Cartesian coordinates, $\mathbf{e}_e$ is the entropy wave eigenvector and $\mathbf{e}_v$ is a linear combination of the vorticity-wave eigenvectors.

As originally developed [5,6], equation (3) did not use the terms in equation (6). Next the terms in equation (6) that use $\mathbf{e}_s$ and $\mathbf{e}_d$ were added [7] to enforce pressure continuity in the cross-flow direction and in the streamwise direction as the Mach number approaches zero. Finally, the terms using $\mathbf{e}_e$ and $\mathbf{e}_v$ were added [8] for flows containing vortices.

Following reference [4], the switches s_l and s_r are defined in the manner of Godunov's method as follows: for $U \geq 0$,

$$\begin{aligned} s_l &= 1 - \epsilon_m \, \epsilon_l \ , \qquad s_r = (1 - \epsilon_m)(1 - \epsilon_r) \ , \\ \epsilon_{l,m,r} &= \frac{1}{2}[\,1 + \mathrm{sign}(M^2_{l,m,r} - 1)] \ , \end{aligned} \tag{7}$$

and M_m denotes the Mach number of the averaged state.

Note that there is current research in improving the sonic point operator [10]. An alternative method to those in reference [10] is: for $U \geq 0$,

$$s_l = 1 - \epsilon_m \, (2\epsilon_l - 1) \ , \qquad s_r = (1 - \epsilon_m)(1 - 2\epsilon_r) \ . \tag{8}$$

This smooth switch is identical to equation (7) except at sonic expansion points. At those points, one- and two-dimensional calculations using equation (8) have shown increased accuracy over equation (7). Equation (8) was derived by modeling a transonic expansion wave for Burger's equation. When the sonic value occurs midway between mesh points, this modeling is exact.

Rotated Differencing

As originally developed, the rotation angle θ used the cosine of the velocity as $\cos\theta = U/q$ when the flow was supersonic. However, it is important to detect whether the velocity projected to the grid line is beyond the Mach cone. Thus, U/q is replaced by $M \cdot U/q = U/c$. If U/c becomes larger than one, $\cos\theta$ is set to one. This enhances the ability to capture oblique shock waves [11].

This feature leads to a favorable resolution of bow and crossflow shocks, but it allows the existence of crossflow expansion shocks. To avoid expansion shocks, the rotation angle is determined by a mixture of averaged (m) and pointwise (l, r) values:

$$\cos^2\theta_{l,r} = \min[\ (1-\phi)\frac{U_m^2}{c_m^2} + \phi\frac{U_{l,r}^2}{c_{l,r}^2},\ 1\ ] \tag{9}$$

The following is used for evaluating ϕ in this paper because of the smoothness:

$$\phi = \max\left(\left(\frac{2\gamma}{\gamma+1}\right)\left\{1 - \frac{1}{2\gamma}[(\gamma-1) + (\gamma+1)\frac{p_2}{p_1}]\right\},\ 0\right), \tag{10}$$

where p_1 and p_2 denote upstream and downstream pressures, respectively. The sine is determined by an arithmetic average of the cosines: $\sin^2\theta = 1 - \frac{1}{2}(\cos^2\theta_l + \cos^2\theta_r)$.

Results

The algorithm given by equation (3) has been tested for flow over a delta wing. Both 2D calculations, using the conical flow approximation [8], and 3D calculations have been made. The calculations are compared with Roe's method [1,2] and central differencing [8] (CD).

Computations are carried out in the following manner. The LU-ADI method [12], which can be modified for the conical flow fields [13], is used for testing the two upwind algorithms as well as the CD algorithm. Each of the three algorithms is implemented explicitly into the LU-ADI method, so that steady flows are determined by each of the three algorithms. Laminar flow is also assumed. For third-order accuracy, the MUSCL scheme with Koren's differentiable limiter [9] is used.

Delta-Wing, Conical-Flow Calculations

This test case considers a vortical flow field over a delta wing in order to examine the present formula's capability for computing shear flows. Computations are done for flow past a 75° delta wing at $M_\infty = 2.8$, $\alpha = 16°$, and $Re = 3.565 \times 10^6$, for which experimental data are available [14]. Figure 1 shows the model geometry, and the typical experimental flow field is shown schematically in figure 2. For the computations, the conical approximation is used. Three grids are used for a grid-refinement study. The coarse, medium, and fine grids all use 51 points normal to the body and 27, 51, and 99 points circumferentially, respectively.

Computations were done with the present method, Roe's method, and the CD method. Figure 3 shows a comparison of density contour plots of three numerical solutions on the fine grids. (The density values are on a portion of the sphere of radius equal to one.) Two shock waves can be observed: one is the bow shock wave on the windward side of the delta wing, and the other is the crossflow shock wave on the leeward side. The present method and Roe's method give similar contour plots for those shock waves, but the CD method gives smeared

plots. (For the CD method, the smoothing coefficient κ was set to 0.1 in the fine-grid case instead of $\kappa = 0.05$ in the other cases because at convergence the solution had numerical oscillations with $\kappa = 0.05$ in the fine grid.) The low density regions at both the primary and secondary vortices also indicate that both upwind methods give similar solutions, but the CD method gives a smeared one.

A comparison of total pressure contour plots on the fine grids is shown in figure 4. The primary vortex appears similar in both upwind solutions, in respect to its location and the contour level, but not in the CD solution. The primary vortex appears off the boundary layer in both upwind solutions, but the primary vortex and the boundary layer touch each other in the CD solution. The shear-flow region separated from the leading edge also shows differences in the three solutions. The present formula gives a sharper solution than Roe's in this shear-flow region. Again, the CD formula gives the most dissipative solution.

Figure 5 shows comparisons of total pressure profiles normal to the leeward surface of the wing at $y = 0.216$ on the coarse, medium, and fine grids. See reference [8] for comparisons at $y = 0.1$, approximately on the primary vortex, and $y = 0.2$, approximately on the secondary vortex. Figure 5(c) shows the main features of the complicated profiles. The first peak near $z = 0$ indicates an edge of the boundary layer under the secondary vortex. The following local minimum corresponds to the secondary vortex. The next peak near $z = 0.025$ indicates the total pressure recovery between the secondary vortex and the shear layer separated from the leading edge. This shear layer from the leading edge is observed as the next local minimum. Finally, the flow recovers to the free stream. The second peak between the secondary vortex and the leading-edge shear layer appears to be higher with respect to both level and location for all three solutions as the grids are refined. The width between the peak and the region of the recovery to the free stream corresponds to the width of the separated shear layer. The present formula gives the narrowest shear layer in the three, even on the fine grid. This crispness indicates that the present formula computes the shear flow most accurately.

Comparisons of pressure coefficient distributions on the leeward wing surface on the coarse, medium, and fine grids are shown in figure 6. Experimental data [14] are also indicated in figure 6 by upper and lower triangles corresponding to data on the right- and left-hand side of the wing, respectively. Results obtained with the present formula are found to be slightly more accurate than those with Roe's method when compared with experimental data as well as with the fine-grid solution. The CD solution has a large discrepancy between the two upwind solutions on the coarse grid, but the discrepancy decreases as the grids are refined.

Finally, a comparison of convergence histories of calculations, using the present and Roe's methods, is shown in figure 7. The locally varying time stepping was used [12]. Because of the stiffness of conical source term, Δt_0 was set to 0.1 in the first 3000 iterations from the impulsive start. Then, $\Delta t_0 = 0.25$ for the next 1000 iterations, and finally Δt_0 was set to 0.5. The maximum CFL number reached about 20. The present formula shows better convergence in both the L_2 norm and the $J \cdot L_\infty$ norm (rescaled by the transformation Jacobian). On the other hand, Roe's formula reaches a limit cycle. The calculations by both upwind methods were started from uniform free-stream conditions. However, the calculations by the CD method were started from a converged solution by the present formula. The CD method needed a smaller Δt_0: that is, one-fifth of the one used for the upwind computations. The present formula converged the best of the three for this shear-flow computation with respect to the convergence rate and the order of magnitude of convergence. The difference in CPU time between the present formula and Roe's formula is less than 1% in the present computations.

Delta-Wing, Three-Dimensional Calculations

A medium-density grid in the curvilinear coordinate system (ξ, η, ζ) was used for calculations for both the present method and Roe's method. There were $25 \times 51 \times 41$ points in the ξ (conical), η (circumferential), and ζ (normal) directions, respectively. The convergence properties were similar to those in the conical-flow calculations. Both methods produce similar results to those obtained in the conical-flow calculations, including the treatment of the bow shock wave and the vortices. Figure 8 shows velocity-magnitude plots at an axial location 90% of the distance from the nose to the trailing edge of the model. First-order accurate results are shown in figure 8(a). The present method (plotted on the right side) shows a slightly larger high-speed region than Roe's method (plotted on the left side). As shown by the third-order results in figure 8(b), this higher speed is more accurate. Hence, the present scheme is less dissipative than Roe's. In this 3D test computation, the CPU time per grid point per iteration is 36.6, 35.7, and 32.1 μsec for the present, Roe's, and CD computations, respectively, on a CRAY X-MP computer. Hence, in 3D, the present method takes about 2.5% more time than Roe's and 14% more time than CD. This confirms that the required arithmetic operations of the present formula are comparable to those of Roe and CD.

Conclusions

An improved streamwise upwind algorithm has been derived and applied to conical flow fields. In comparison with Roe's method, the present formula (1) captures oblique shock waves in the same manner, (2) requires arithmetic operations of the same order, (3) has better convergence properties, i.e., no limit cycle, and (4) has an advantage over Roe's in computing shear flows accurately. The results also indicate that the CD method is more dissipative in the resolution of shock waves and shear layers than upwind methods. In addition, the present method switches differencing at sonic values rather than at values that are dependent on the coordinate system, which is more in accord with the fluid physics.

References

[1] Roe, P. L.: "Characteristics-based schemes for the Euler equations," *Ann. Rev. Fluid Mech.*, 18, 1986, pp. 337-65.

[2] van Leer, B., Thomas, J. L., Roe, P. L., Newsome, R. W.: "A comparison of numerical flux formulas for the Euler and Navier-Stokes equations," AIAA Paper 87-1104-CP, Proc. AIAA 8th Comp. Fluid Dynamics Conf., Honolulu, June 1987.

[3] Vatsa, V. N., Thomas, J. L., Wedan, B. W.: "Navier-Stokes computations of prolate spheroids at angle of attack," AIAA Paper 87-2627-CP, Aug. 1987.

[4] Jameson, A.: "Transonic potential flow calculations in conservation form," Proc. AIAA 2nd Comp. Fluid Dynamics Conf., Hartford, Conn., June 1975, pp. 148-161.

[5] Goorjian, P. M.: "Algorithm development for the Euler equations with calculations of transonic flows," AIAA Paper 87-0536, Jan. 1987.

[6] Goorjian, P. M.: "A new algorithm for the Navier-Stokes equations applied to transonic flows over wing," AIAA Paper 87-1121-CP, Proc. AIAA 8th Comp. Fluid Dynamics Conf., Honolulu, June 1987.

[7] Goorjian, P. M.: "A streamwise upwind algorithm for the Euler and Navier-Stokes equations applied to transonic flows," *Numerical Methods for Fluid Dynamics III*, Inst. Mathematics & Appl. Conf. Series, New Series No. 17, Clarendon Press, Oxford, 1988.

[8] Obayashi, S., Goorjian, P. M.: "Improvements and applications of a streamwise upwind algorithm," AIAA Paper 89-1957-CP, Proc. AIAA 9th Comp. Fluid Dynamics Conf., pp. 292-302, June 1989.

[9] Obayashi, S., Gavali, S.: "Three-dimensional simulation of underexpanded plumes using upwind algorithms," *Supercomputing 88, II: Science and Applications*, pp. 25-33, IEEE Computer Society Press, Washington, D.C., 1989.

[10] van Leer, B., Lee, W.-T., Powell, K. G.: "Sonic-point capturing," AIAA Paper 89-1945-CP, Proc. AIAA 9th Comp. Fluid Dynamics Conf., pp. 176-187, June 1989.

[11] Albone, C. M., Hall, M. G.: "A scheme for the improved capture of shock waves in potential flow calculations," RAE TR 80128, Oct. 1980.

[12] Obayashi, S.: "Numerical simulation of underexpanded plumes using upwind algorithms," AIAA Paper 88-4360-CP, Aug. 1988.

[13] Fujii, K., Obayashi, S.: "Evaluation of Euler and Navier-Stokes solutions for leading-edge and shock-induced separations," AIAA Paper 85-1563, June 1985.

[14] Miller, D. S., Wood, R. M.: "Lee-side flow over delta wings at supersonic speeds," NASA TP-2430, June 1985.

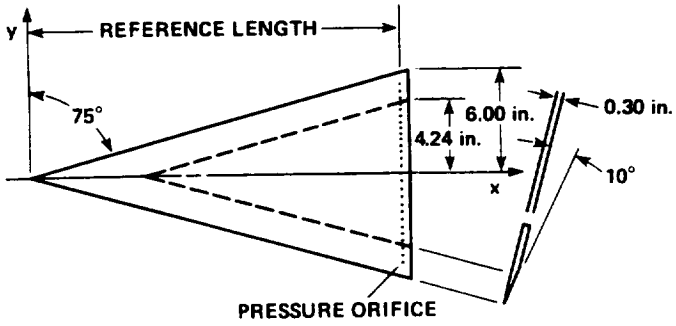

Fig. 1 Model geometry.

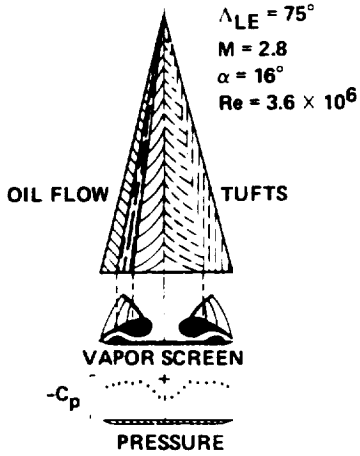

Fig. 2 Experimental flow field of vortex with shock wave (ref. 14).

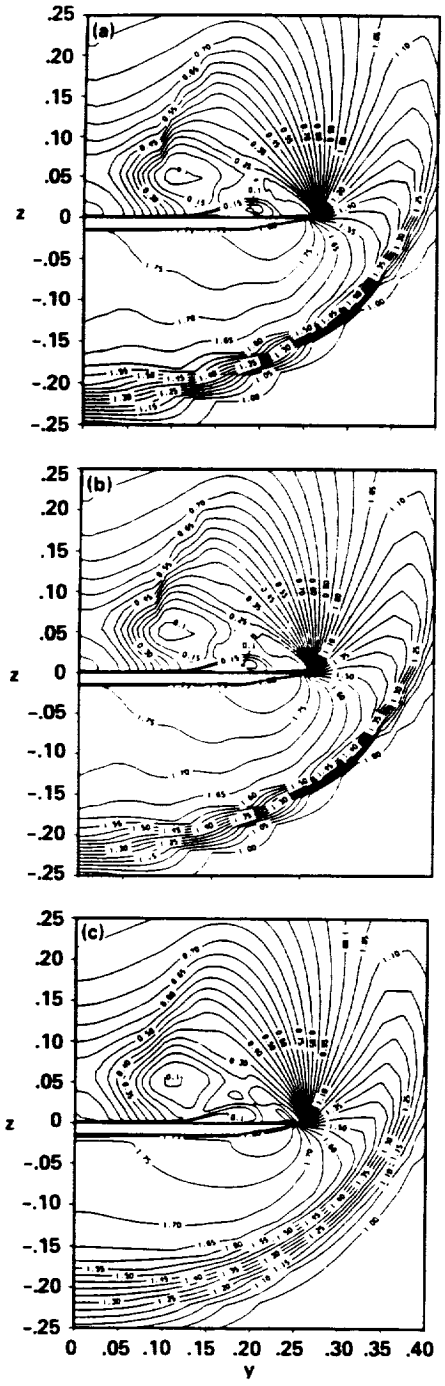

Fig. 3 Comparison of density contour plots on the fine grid; $M_\infty = 2.8$, $Re = 3.565 \times 10^6$, $\alpha = 16°$. a) the present formula; b) Roe's formula; c) the central-difference method.

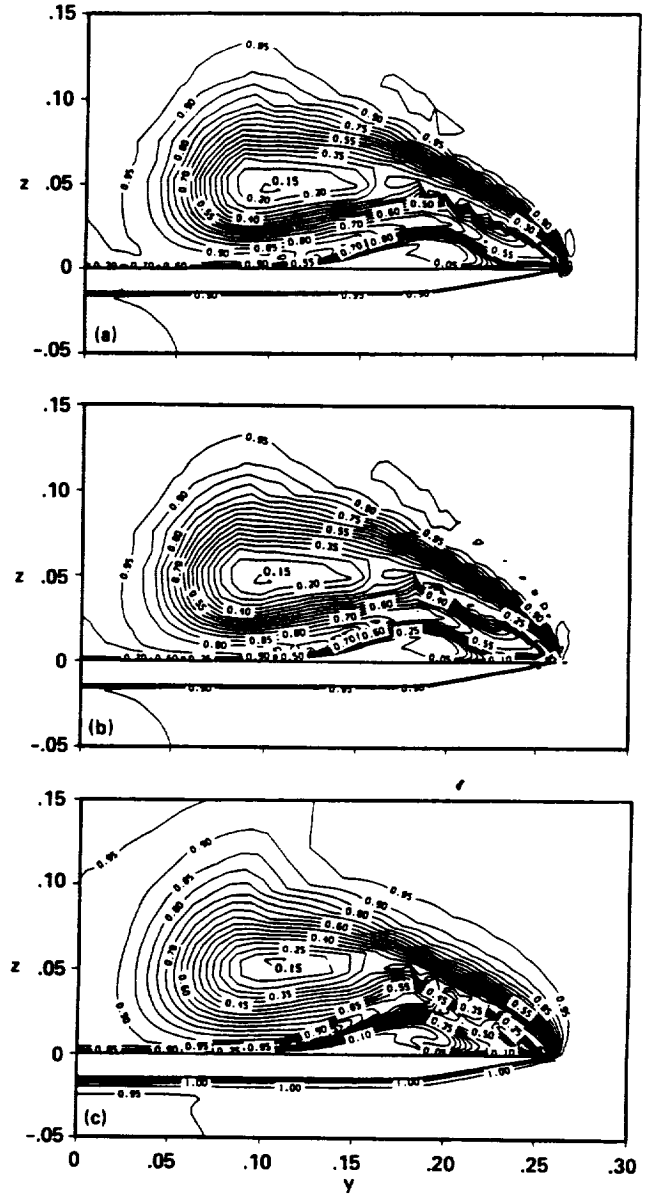

Fig. 4 Comparison of total pressure contour plots on the fine grid; $M_\infty = 2.8$, $Re = 3.565 \times 10^6$, $\alpha = 16°$. a) the present formula; b) Roe's formula; c) the central-difference method.

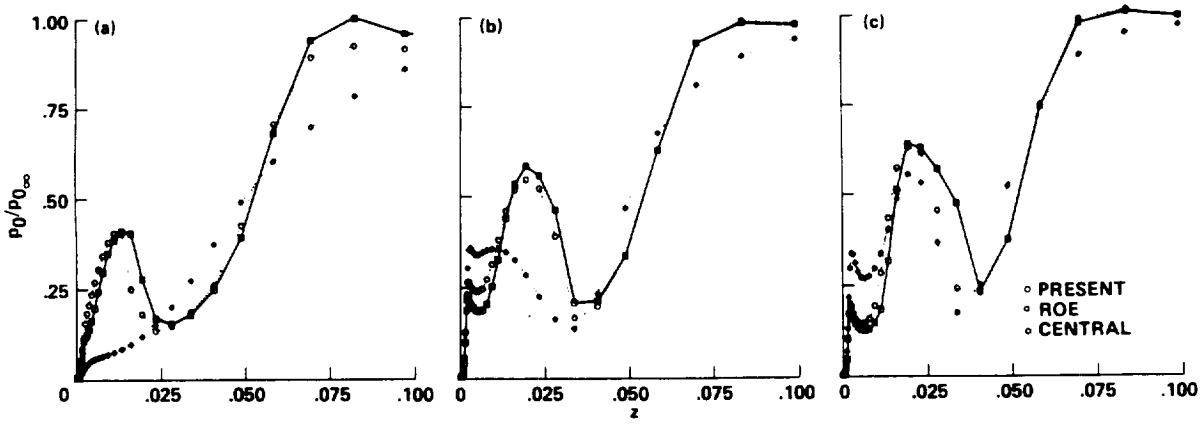

Fig. 5 Comparisons of total pressure profiles at $y = 0.216$. a) coarse grid; b) medium grid; c) fine grid.

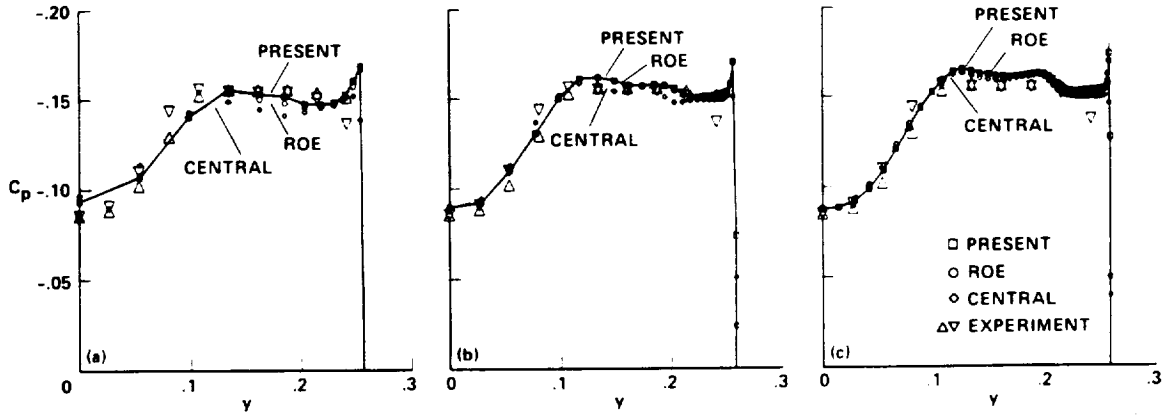

Fig. 6 Comparisons of C_p distributions on the leeward wing surface. a) coarse grid; b) medium grid; c) fine grid.

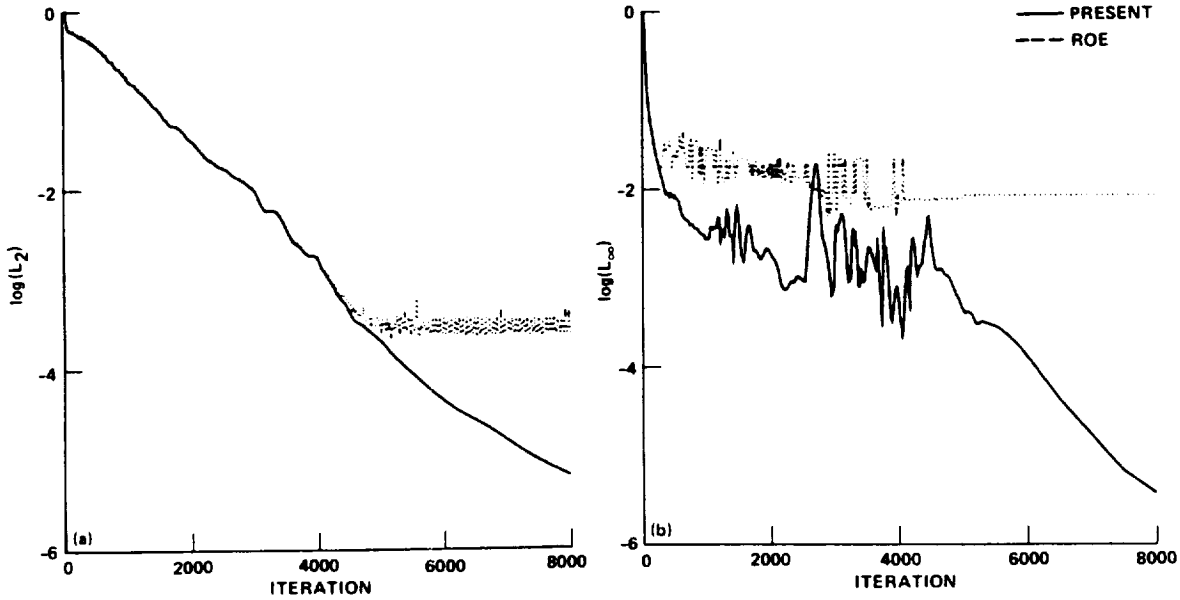

Fig. 7 Comparisons of convergence history on the medium grid. a) L_2 norm; b) $J \cdot L_\infty$ norm.

ORIGINAL PAGE IS
OF POOR QUALITY

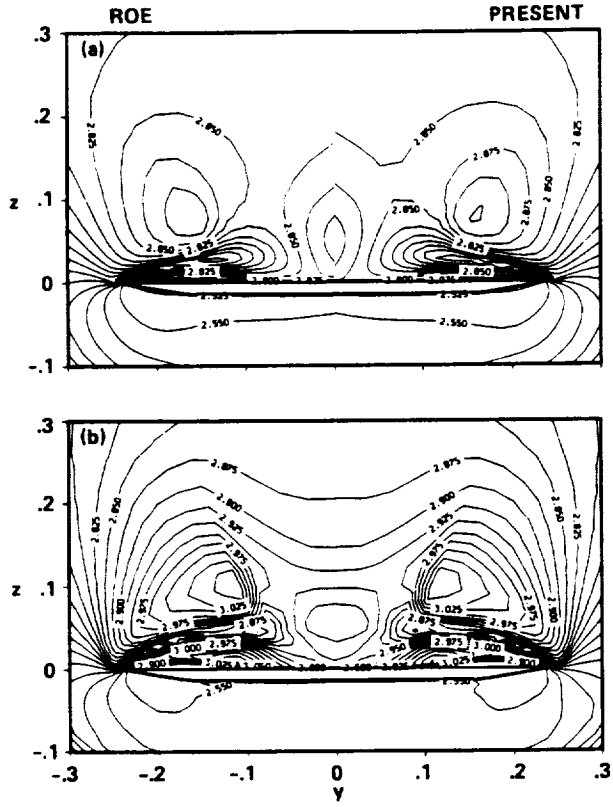

Fig. 8 Comparisons of velocity magnitude contour plots. a) first-order; b) third-order.

NASA
National Aeronautics and Space Administration

Report Documentation Page

1. Report No.	2. Government Accession No.	3. Recipient's Catalog No.
NASA TM-102225		

4. Title and Subtitle
A Streamwise Upwind Algorithm Applied to Vortical Flow over a Delta Wing

5. Report Date
October 1989

6. Performing Organization Code

7. Author(s)
Peter M. Goorjian and Shigeru Obayashi

8. Performing Organization Report No.
A-89230

10. Work Unit No.
505-60

9. Performing Organization Name and Address
Ames Research Center
Moffett Field, CA 94035

11. Contract or Grant No.

13. Type of Report and Period Covered
Technical Memorandum

12. Sponsoring Agency Name and Address
National Aeronautics and Space Administration
Washington, DC 20546-0001

14. Sponsoring Agency Code

15. Supplementary Notes
Point of Contact: Peter M. Goorjian, Ames Research Center, MS 258-1, Moffett Field, CA 94035
(415) 694-5547 or FTS 464-5547
Presented at the Eighth GAMM Conference on Numerical Methods in Fluid Mechanics, Sept. 27-29, 1989, Delft, Netherlands.

16. Abstract

Improvements have been made to a streamwise upwind algorithm so that it can be used for calculating flows with vortices. A calculation is shown of flow over a delta wing at an angle of attack. The laminar, thin-layer, Navier-Stokes equations are used for the calculation. The results are compared with another upwind method, a central-differencing method, and experimental data. The present method shows improvements in accuracy and convergence properties.

17. Key Words (Suggested by Author(s))	18. Distribution Statement
Computational fluid dynamics, Numerical methods, Upwind methods, Vortical flow, Vortical flow over a delta wing	Unclassified-Unlimited Subject Category - 02

19. Security Classif. (of this report)	20. Security Classif. (of this page)	21. No. of Pages	22. Price
Unclassified	Unclassified	11	A02